

**RADIATIVE IGNITION AND TRANSITION TO SPREAD
INVESTIGATION (RITSI)**

by

**Takashi Kashiwagi
Building and Fire Research Laboratory
National Institute of Standards and Technology
Gaithersburg, MD 20899, USA**

and

**Sandra L. Olson
Lewis Research Center
Cleveland, OH 44135, USA**

**Reprinted from the Third United States Microgravity Payload: One Year Report.
Proceedings. February 10-11, 1997, Washington, DC, 97-117 pp, 1998.**

**NOTE: This paper is a contribution of the National Institute of Standards and
Technology and is not subjected to copyright.**

RADIATIVE IGNITION AND TRANSITION TO SPREAD INVESTIGATION (RITSI)

Takashi Kashiwagi
Building & Fire Research Laboratory
NIST
Gaithersburg, MD 20899

Sandra L. Olson
Lewis Research Center
NASA
Cleveland, OH 44135

Phone: 301-975-6699
FAX: 301-975-4052
email: takashi.kashiwagi@nist.gov

216-433-2859
216-433-8660
sandra.olson@lerc.nasa.gov

Abstract

A total of 25 experiments was conducted in the Glovebox Facility on the USMP-3 mission to study the behavior of both flaming and smoldering ignition events, the transition from ignition to flame/smoldering spread, and the flame/smoldering growth pattern in air. Twenty-one of the 25 experiments were flaming experiments and the remainder were smoldering experiments. Ignition was initiated by a heated wire across a thermally thin filter paper in the middle of the sample for the two-dimensional configuration and by a focused beam from a halogen/tungsten lamp at the center of the sample for the three-dimensional configuration. The external air flow velocity was varied from 0 cm/s to 6.5 cm/s. The ignition and subsequent flame spread events were recorded by a video camera, a 35 mm camera, and 6 thermocouples (2 in the gas phase and 4 in the sample). The results indicate that non-piloted radiative ignition of the paper by external thermal radiation tends to occur more easily than in normal gravity. In the two-dimensional configuration, the transition from ignition to downstream flame spread never occurred; only the transition to upstream spread took place. In the three-dimensional configuration, a char growth pattern emerged in the shape of a fan, with the ignited area as the center of the fan and the fan spreading in the upstream direction. The internal angle of the fan increased with an increase in external flow velocity (higher flow velocity gave a more opened fan pattern). At an external flow velocity of 5 cm/s, the flame was horseshoe-shaped and the char pattern became an elongated semicircle toward upstream. It appears that the peak upstream flame spread rate was reached at a higher external velocity than for the two-dimensional flame front. Flame spread much faster along open edges of the sample paper than along the sample face, presumably due to there being larger supply of oxygen and energy feedback at the open edges than at the surface. These results indicate the possible importance of the effect of the flame front shape such as the curvature of the flame front on spread rate and flame strength. A complex, unexpected finger-shaped char growth pattern was observed during the smoldering experiment. Higher external flow velocity increased the number of localized smoldering fronts, of the char fingers they left behind, and frequency of bifurcations from the fingers. At present, it is not clear what caused such a complex char growth pattern .

Introduction

Ignition of solid fuels by external thermal radiation and subsequent transition to flame spread are processes that not only are of considerable scientific interest but which also have fire safety applications. The fire safety strategy in a spacecraft is (1) to detect any fire as early as possible, (2) to keep any fire as small as possible, and (3) to extinguish any fire as quickly as possible^[1,2]. This suggests that a material which undergoes a momentary ignition might be tolerable but a material which permits a transition to subsequent flame spread would significantly increase the fire hazard in a spacecraft. If the transition does not take place, then by definition flame spread does not occur. Therefore, the limiting condition under which flame cannot spread should be calculated from a model of the transition from ignition instead of by the traditional approach based on limits to a steady flame spread model. However, although the fundamental processes involved in ignition have been suggested^[3,4,5,6], there have been no definitive experimental or modeling studies due to the flow motion generated by buoyancy near the heated sample surface. One must solve the time-dependent Navier-Stokes equations over an extended region to represent the highly unstable buoyant plume accurately. It is especially important to provide correct far-field boundary conditions, particularly velocities. This is also important during the transition period from ignition to flame spread but there has been hardly any previous work on this transition.

Almost all previous works have studied ignition and flame spreading separately^[7,8]. In order to avoid the specification of the boundary conditions, previous detailed radiative ignition models were assumed to be one-dimensional^[9,10,11] or were applied at a stagnation point^[12]. The mismatch between experimental and calculated geometries in normal gravity means that theories cannot be compared directly with experimental results except for specific configurations under which the plume is not formed. In previous flame spread studies, time-dependent flame spread models are limited to upward flame spread over a vertically oriented material surface in normal gravity and is generally assumed to be two-dimensional. Almost all detailed flame spread models^[7,8,13] were based on the steady-state flame spread rate and, as far as we are aware, there are no previous studies of three-dimensional time-dependent flame spread which is initiated from a small, localized ignited area. This scenario is most common in real fires. The mechanism of the transition from ignition to flame spread also controls the extinction limit of flame spread, which is affected by the flame history, starting at ignition. Since this is an inherently transient process, conventional approaches analyzing the steady-state flame spread near its extinction limit cannot truly reveal the dynamic aspects of the transition. Modeling of the transition from ignition to flame spread is extremely difficult in a normal gravity environment. Thus, the study of localized ignition and the subsequent transition to flame spread in a three-dimensional configuration in a microgravity environment is needed to obtain new information for understanding transition mechanisms.

Smoldering (non-flaming glowing combustion) is one of the common modes of initiation of fires; it might provide potentially hazardous conditions due to its high CO yield, but there are only a limited number of studies available. Therefore, its detailed mechanism is not fully understood. Although the heat release rate from smoldering is smaller than that from flaming, the temperature of the smoldering front is as high as 800 °C or more and the induced buoyant

flow from the high temperature smoldering front cannot be neglected in normal gravity. The induced buoyant flow makes it extremely difficult to quantify and control the supply rate of oxygen to the smoldering front in normal gravity. Since the supply of oxygen to the smoldering front is one of the critical parameters which control smoldering spread rate, it is extremely difficult to predict the effects of slow external flow on smoldering behavior and its spread rate over a cellulosic surface.

1. Experimental Objectives

The Radiative Ignition and Transition to Spread Investigation experiment (RITSI) was designed to obtain test data on the following phenomena:

- (1) Observe and measure the effects of low external flow velocity similar to ventilation velocities in a spacecraft on flaming ignition, transition, and flame growth pattern over a thin cellulosic paper surface in the two-dimensional configuration and also in the three-dimensional configuration.
- (2) Observe and measure flame spread along open edges and corner of thin paper at different external low flow velocities.
- (3) Observe and measure the effects of low external flow velocity on the growth pattern of smoldering from localized smoldering ignition.

To make these observations, 15 experiments were planned with an additional 10 samples as extra if added experimental time became available. Fortunately, all 25 tests could be conducted over three days; the tests conditions are listed in Table 1. 15 tests were conducted for item (1), 6 tests were for item (2), and 4 tests were for item (3).

2. Experimental Hardware and Operations

RITSI USMP-3 Glovebox experiment hardware, shown in Figure 1, consists of two experimental modules, a control box, a display box, and two parts boxes, which house the fifteen individual sample boxes and other miscellaneous supplies, including 10 additional fuel samples. One sample box is shown opened to reveal the sample card, product filter, and cleaning supplies (not visible) stowed inside. The small external control box (which attaches to the outside of the Glovebox front door) include fan on/off and variable speed control, ignitor wire activation radiant heater activation and variable power adjustment, and chamber light on/off switch.

Each experimental module, shown schematically in Figure 2, uses a small fan to generate a low flow velocity of up to 6.5 cm/s through the test section. The test section was 85 mm wide x 95 mm high x 171 mm long. The transparent lid of the duct opens for access to change sample cards. A filter downstream of the combustion event collects particulates and other combustion

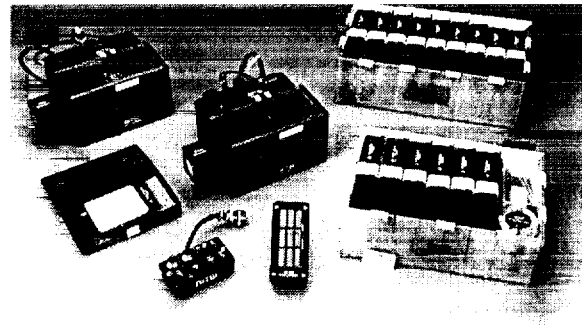


Figure 1 RITSI hardware picture (two modules, two sample/holder storage containers, one sample/holder, electronic control, and outputs display)

products.

A near-infrared tungsten/halogen radiant heater is used to ignite most samples, and is recessed into the back wall of the duct to minimize disturbances to the flow, as also shown schematically in Figure 2. The power to the lamp was measured during each test. The lamp automatically deactivated at a preset time. The emission spectrum of the lamp was measured from 2 to 20 μm using a FTIR.

A sample card is shown in Figure 3. A 10 cm x 8.7 cm sheet of Whatman 44¹ ashless filter paper was used as the sample. The center part of the sheet over the irradiated area was blackened to increase absorption of the incident beam from the lamp. The absorptivity of the blackened paper was measured by the NIST radiometric group between 1 and 20 μm . The samples were ignited at a central location either by the focused beam from the lamp (three-dimensional configuration) or along a line by a heated wire to observe planar flame growth (two-dimensional configuration). A few samples were doped with a smolder promoting agent, potassium acetate, to study smolder propagation from a central ignition point. Six 0.05 mm diameter type K thermocouples and an ignitor wire (30 gauge Kanthal wire) were pre-installed across the sample on each sample holder. Four thermocouples were installed in the sample at the center, 2 cm and 4 cm downstream from the center and at 2 cm upstream. Two thermocouples were installed at 2 mm above the sample surface at 2 cm upstream and also downstream locations from the center. The thermocouple data were recorded along with radiant

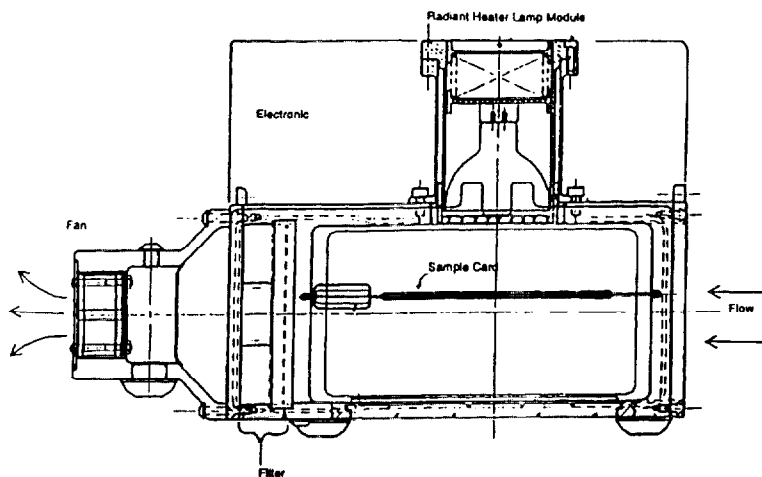


Figure 2 Schematic cross section view of hardware

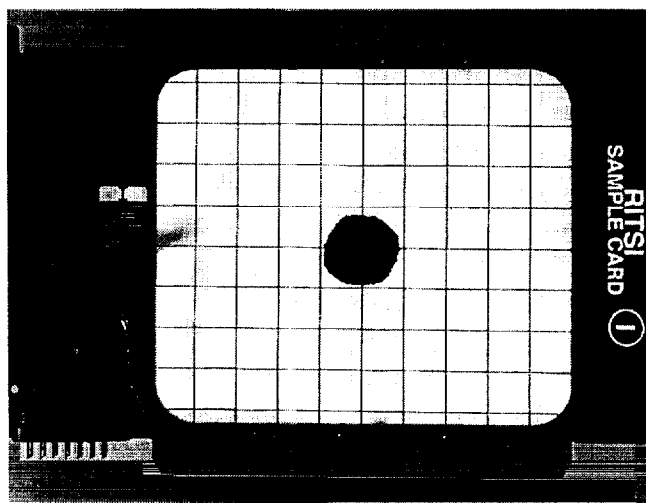


Figure 3 Sample card with 1 cm by 1 cm grid

¹Certain company products are mentioned in the text in order to specify adequately the experimental procedure and equipment used. In no cases does such identification imply recommendation or endorsement by the National Institute of Standards and Technology and NASA, nor does it imply that the products are necessarily the best available for the purpose.

heater power, ignitor power, and flow velocity.

Color video pictures were taken in the direction normal to the sample surface to view changes in the flame shape and char pattern. Red diodes were used to illuminate the sample surface. Still color photographs were taken at an oblique angle to the sample by a motor-driven 35 mm camera. The flaming tests require the use of a blue transmitting/red blocking top window to observe the dim flame through the near-IR lamp light being scattered by the smoke, in addition to the red LED light being scattered. A window transmissive throughout the visible was used to image the smoke patterns for the smoldering tests.

The test matrix is given in Table 1. The first fifteen tests were instrumented with thermocouples; the last ten were assembled in orbit without thermocouples using the spare sample materials flown.

3. Test Results and Discussion

3.1 Ignition

Ignition was achieved in almost all tests using either a heated wire or a lamp. Since radiative ignition was not achieved with the same system in normal gravity, it was initially planned that a heated wire above the irradiated sample surface would be used as a pilot during the lamp irradiation if ignition was not achieved in the first radiative ignition test without the heated wire. Surprisingly, however, ignition was achieved without using a heated wire in the first test, and all tests in the three-dimensional configuration were ignited by the lamp alone. It appears that in normal gravity, hot combustible degradation products were cooled and swept away from the hot irradiated surface due to buoyancy-induced flow and non-piloted ignition was thus difficult to achieve in normal gravity. In microgravity, however, the hot combustible degradation products tended to stay near the irradiated surface (expansion and diffusion are the only mechanisms which cool and slowly move the products away from the irradiated area) and non-piloted ignition (self-induced pilot from the hot irradiated surface) tended to occur compared to the case in normal gravity. Radiative ignition by the lamp was quite reproducible and preliminary results show that the ignition delay time (a little over 4 s after the ignition switch was turned on) was nearly constant in the range of flow velocities used in this study. This ignition delay time included about 2.2 s from power on to a point where the output of the lamp reached the designated flux. Ignition by a heated wire was less reproducible than that by the lamp due to changes in wire contact with the sample caused by the expansion of the wire after it heated. Ignition tended to occur at one face of the sample surface at first followed by the second ignition on the other face of the sample surface.

3.2 Transition and Growth of Flame and Char Pattern

3.2.a Two-dimensional Configuration

Four tests were conducted at the external flow velocities of 0, 2, and 5 cm/s. The behavior of the flame from the side view parallel to the paper sample is shown in Figs 4 for the three different

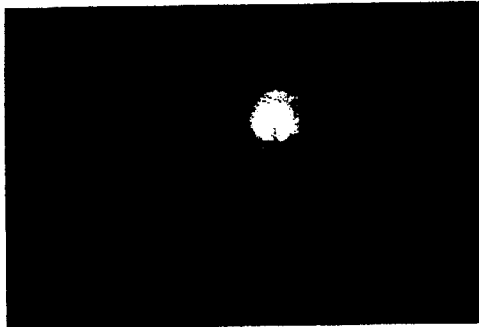


Figure 4a: quiescent ignition

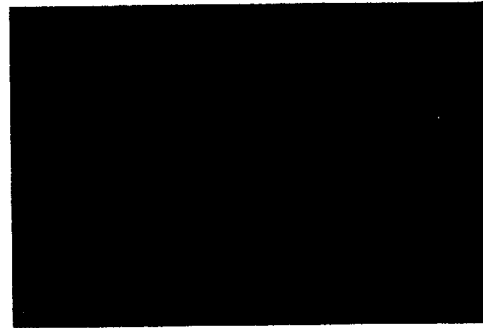


Figure 4b: quiescent transition

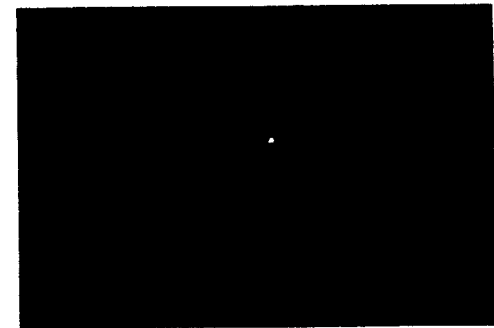


Figure 4c: quiescent extinction



Figure 4d: 2 cm/s ignition

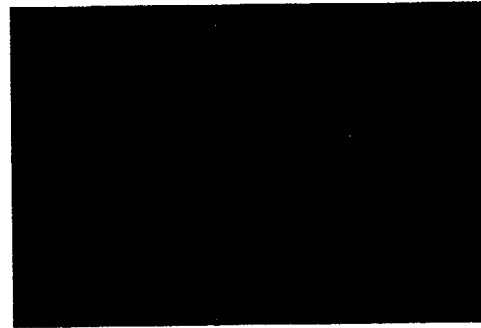


Figure 4e: 2 cm/s transition

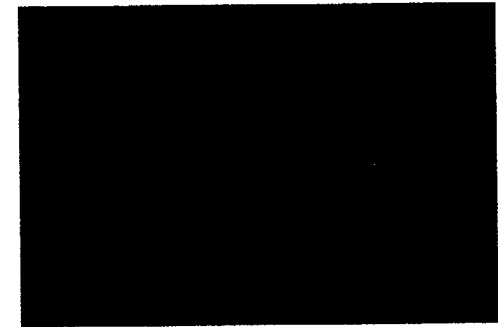


Figure 4f: 2 cm/s flame spread



Figure 4g: 5 cm/s ignition



Figure 4h: 5 cm/s transition

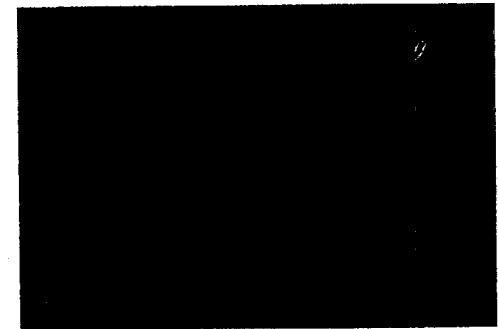


Figure 4i: 5 cm/s flame spread

Figure 4 Flame spread at three different flow velocities in two-dimensional configuration (Flow from right)

flow velocities at three different stages: ignition, transition to flame spread, and fully developed flame spread. At ignition, Figs. 4a, 4d, and 4g, a blue flame appeared only over one face of the sample surface due to the contact condition of the expanded heated wire with the sample as discussed above. In the quiescent condition, Fig. 4a, an orange glow appeared over the other face of the sample surface. This glow was caused by the scattered light from the glowing heated wire by degradation products from the paper sample; it was not flame. This glow died and only the bottom side of the flame persisted, as shown in Fig. 4b. Nevertheless, a much fainter scattered vapor cloud can still be seen in this figure. At the later stage, Fig. 4c, the bottom flame disappeared leaving a faint vapor cloud similar to the that over the other face of the sample surface; the transition from ignition to flame spread did not occur. These clouds indicate that there might be enough combustible degradation products in the gas phase close to the heated wire to ignite but it appears that oxygen supply was not sufficient to yield ignition. At 2 cm/s and 5 cm/s, flames appeared on both sides of the sample surface and the flames continued to spread upstream to the end of the sample. This observation suggests that flames over both sides of the sample surfaces might be needed for the transition to flame spread and the supply of oxygen appears to be the rate-controlling process to transition to flame spread. The observed upstream flame spread has been predicted in our theoretical calculation^[14] and the overall shape of the spreading flame calculated in this reference is very similar to that seen in these figures. The flame became longer with an increase in the external flow velocity and the color of the flames remained blue in the range of the flow velocities used in this study.

Selected video pictures normal to the sample surface in the two-dimensional configuration are shown in Figs. 5. Since the blue color of the flames was faint, only the growth pattern of the char layers (faint dark color) can be seen in these figures. Careful observation reveals that a spreading blue flame front was several millimeters ahead of the char front. This is also confirmed by an earlier temperature increase 2 mm above the sample surface than the temperature increase in the sample at a location 2 cm upstream from the center of the irradiated area, as shown in Fig. 6. The figure shows a rapid sample temperature increase at the center of the irradiated area up to about 450 °C; it stayed at this temperature even when the lamp was turned off at about 6 s. After about 8 s, this temperature started to increase gradually up to almost 700 °C, presumably due to glowing (smoldering) of the char. The increase in sample temperature at two downstream locations (2 cm and 4 cm from the irradiated center) occurred at earlier time than that at 2 cm in the upstream but its rate of increase in the downstream location was much less than that in the upstream location. This indicates that hot combustion products were swept downstream shortly after the onset of ignition but the sample temperature at the 2 cm downstream location was not high enough, only up to about 200 °C till 10 s and later up to about 250 °C, to generate char. Even the gas phase temperature at 2 mm from the surface at the 2 cm downstream location went up to only about 400 °C compared to above 800 °C at the 2 cm upstream location. At the 4 cm downstream location, the sample temperature increases up to only about 150 °C. It is expected that at least 300 °C is needed to form char for this sample^[15]. Therefore, the char layer growth was observed only in the upstream side at 2 and 5 cm/s flow velocities. With the measured sample temperature history during the approaching flame front (fitting with a linear temperature increase with time), the net energy feedback rate (total feedback rate minus radiative/convective losses from the sample surface) from the upstream spreading flame front to the sample at the 2 cm upstream position and also those from hot combustion

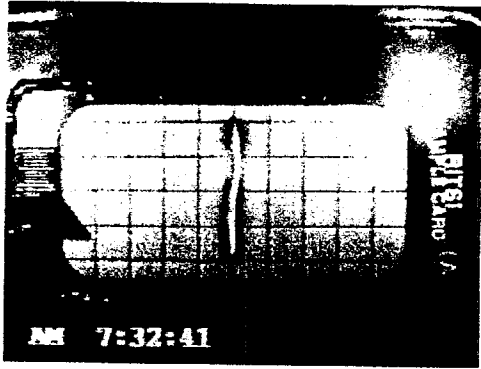


Figure 5a: quiescent ignition

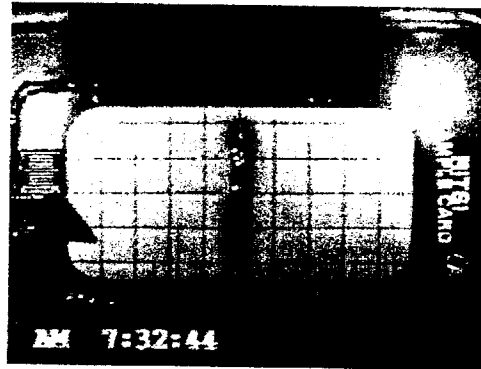


Figure 5b: quiescent transition

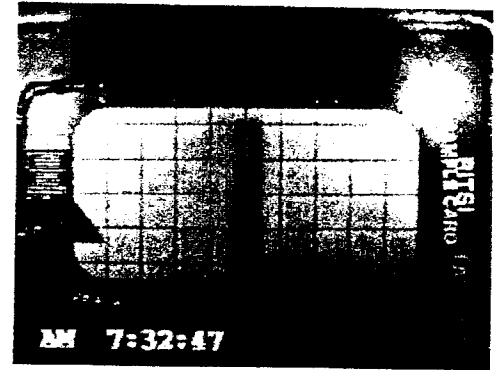


Figure 5c: quiescent extinction

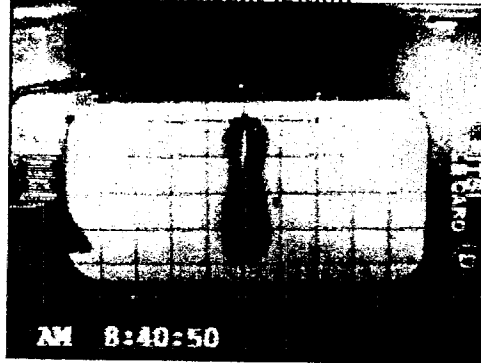


Figure 5d: 2 cm/s after ignition

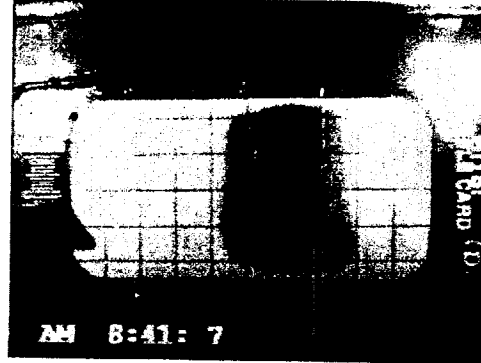


Figure 5e: 2 cm/s spread

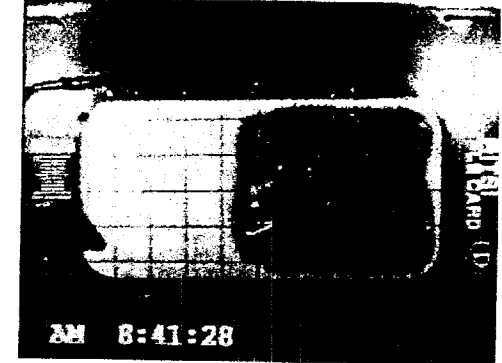


Figure 5f: 2 cm/s fully spread

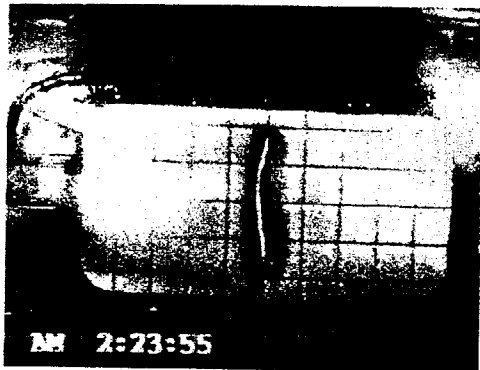


Figure 5g: 5 cm/s after ignition

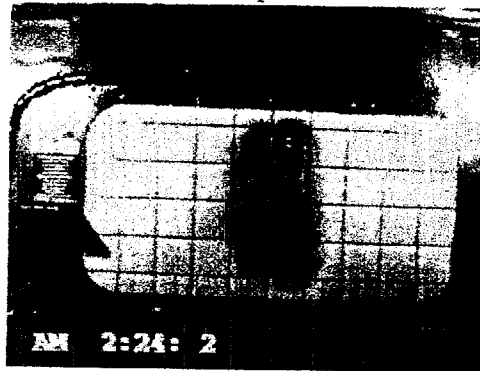


Figure 5h: 5 cm/s spread

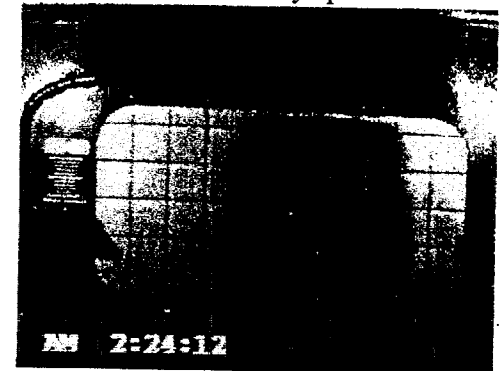


Figure 5i: 5 cm/s nearly fully spread

Figure 5 Char growth patterns at three different flow velocities in two-dimensional configuration (Flow from right).

products flow at 2 cm and 4 cm downstream locations were calculated. In the calculation it was assumed that the sample was thermally thin and the flame and the flow were symmetric about the sample; the net energy feedback rate from the upstream flame is $3.3 \text{ W/cm}^2 \pm 10\%$ for each surface (top and bottom), that from the hot products flow at the 2 cm downstream location is $0.6 \text{ W/cm}^2 \pm 10\%$ for each surface and that at the 4 cm downstream location is $0.2 \text{ W/cm}^2 \pm 10\%$ for each surface.

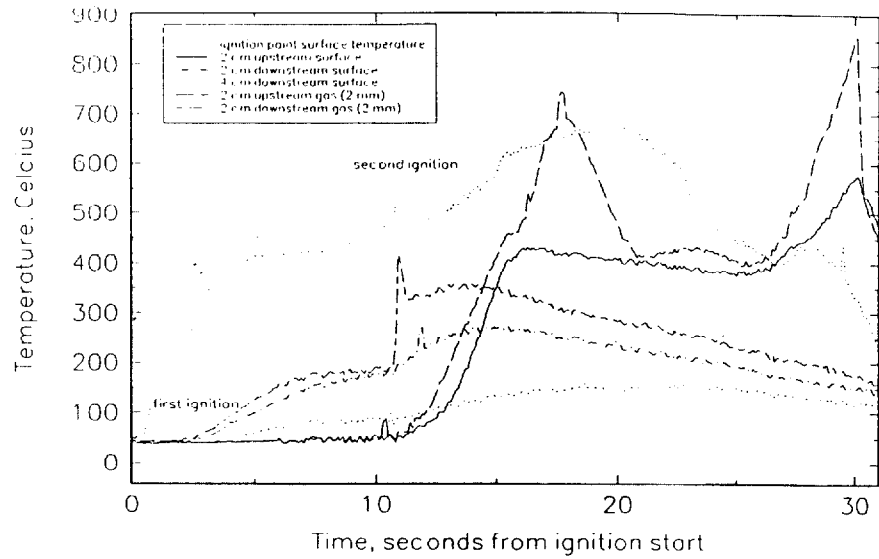


Figure 6 Temperature histories in two-dimensional configuration, 5 cm/s

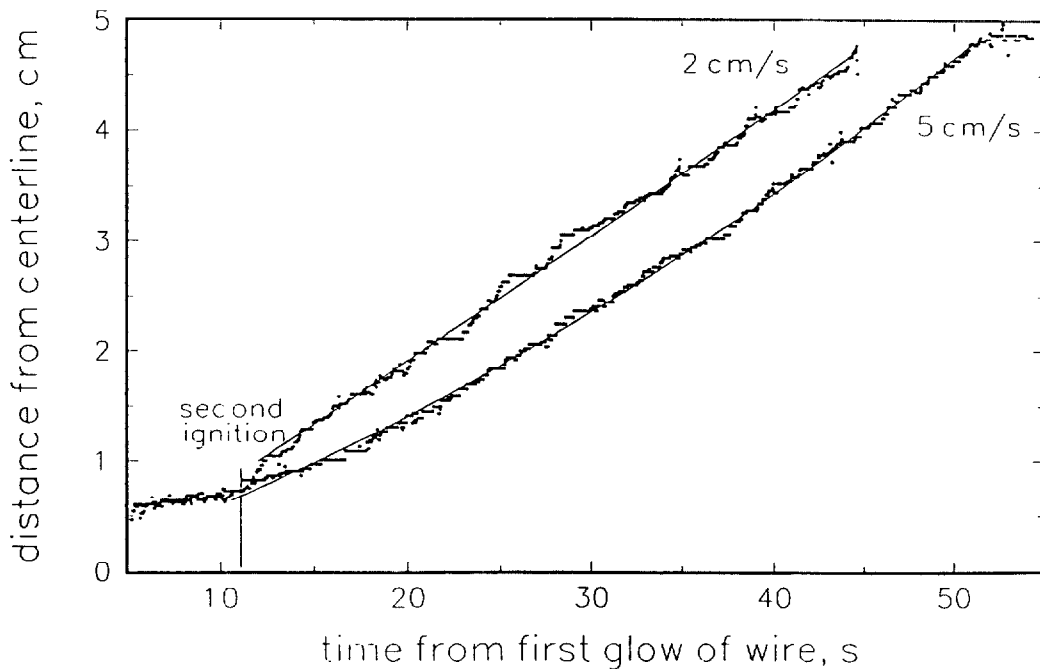


Fig. 7 Upstream char-front location histories in two-dimensional configuration.

Since the flame was faint and hard to see clearly in the recorded videos, the growth of the char patterns shown in Figs. 5 was used to calculate char spread rate. As the distance between the spreading char front and traveling flame front appeared to be nearly constant, it was assumed that

the char spread rate was the same as flame spread rate. The position of the char front spreading toward upstream was measured at different times for the external flow velocities of 2 cm/s and 5 cm/s; the results are plotted in Fig.7. As shown in this figure and discussed above, the flame hardly spread when only one side of the sample was ignited. After the second ignition at the side opposite from the first ignition, the flames started to spread. At 2 cm/s, it appears that char spread at an apparently steady rate shortly after the second ignition but at 5 cm/s, initially char spread slowly and then reached the apparently steady rate. Both apparently steady char spread rates are about the same; they were 0.11 ± 0.01 cm/s. Since the char spread rate for the case of 5 cm/s appears to increase with an increase in distance from the ignited area, as shown in Fig.7, some caution is needed for the spread value at an external flow velocity of 5 cm/s.

3.2 b Three-dimensional Configuration

Although flaming ignition was observed in the quiescent condition, transition to flame spread did not occur. However, that transition did occur at external flow velocities of 0.5 cm/s, 1 cm/s, 2 cm/s, 3.5 cm/s, 5 cm/s and 6.5 cm/s. The growth patterns of flame for the 0.5 cm/s, 2 cm/s, and 6.5 cm/s cases are shown in Figs. 8. These pictures were taken by a 35 mm camera looking downward at an oblique angle. The color of the flames was blue during the experiments, similar to the above cases for the two-dimensional configuration. At 0.5 cm/s, a small flame spread only upstream maintaining the initial flame shape from shortly after ignition. The flame never grew laterally from the initial width and this is also clearly seen in the growth pattern of char in Figs. 9a-c. However, the flame and char growth patterns did grow laterally outward with an increase in the external velocity, as shown in Figs. 8 and 9. At 2 cm/s, the flame had a crescent shape and the char growth pattern was initially an elongated circle pointing upstream; at later times, it became fan-shaped. At 6.5 cm/s, the shape of the flame became like a horseshoe with the tails of the horseshoe flame extending downstream. The char pattern became an elongated circle in the upstream direction with a relatively flat downstream side. A similar shape was also observed in 35% and 50% oxygen concentrations at 5 cm/s external flow velocity^[16], although the color of these flames was orange. Our theoretical calculations predicted a similar shape of flame at 5 cm/s^[16]. A major difference in flame shape between air in this study and 50% oxygen concentration is that a spreading spherical flame was observed in a quiescent condition in 50% oxygen concentration compared with no transition to flame spread in the air case. Therefore, at low external velocities, the char patterns were more or less spherical in 50% oxygen concentration instead of the narrow strip char pattern observed in the air case. The observed trend of opening the angle of the char pattern in the upstream direction with an increase in external flow velocity of air in microgravity is quite different from the narrowing angle trend of the downstream flame with an increase in external flow velocity in normal gravity. However, it is expected that further increase in external velocity in microgravity would eventually reduce upstream flame spread rate and be sufficient to promote downstream flame spread. Thus, this observed trend of the char pattern is unique and should occur only at low external flow velocities and low oxygen concentrations, such as in air, in microgravity.

The sample temperatures were measured along the center line at four locations; one was at the center of the irradiated area, one was at the 2 cm upstream location, and two were at 2 cm and 4 cm downstream locations. The gas-phase temperatures were measured 2 mm above the sample surface at the 2 cm downstream location and at the 2 cm upstream location. The results for an

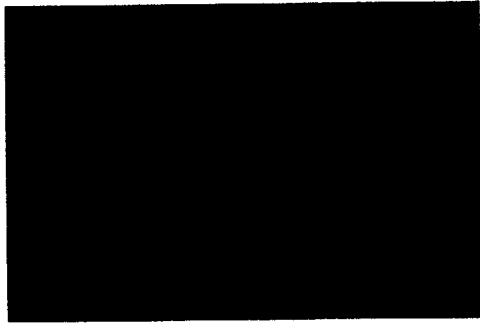


Figure 8a: 0.5 cm/s after ignition

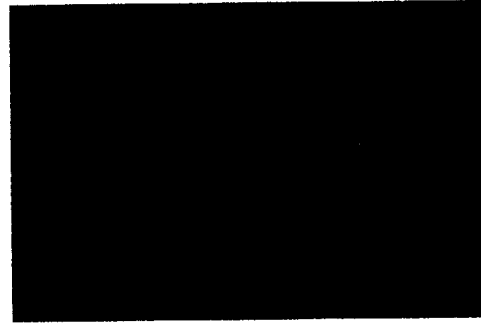


Figure 8b: 0.5 cm/s spread

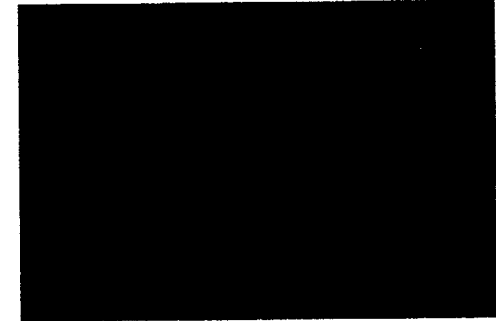


Figure 8c: 0.5 cm/s full spread

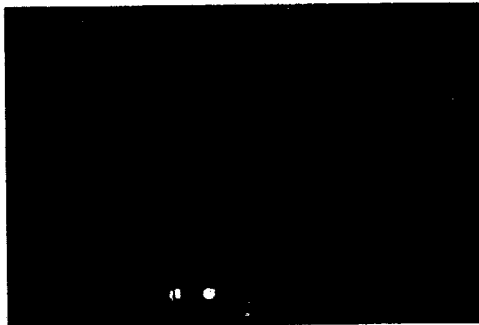


Figure 8d: 2 cm/s after ignition

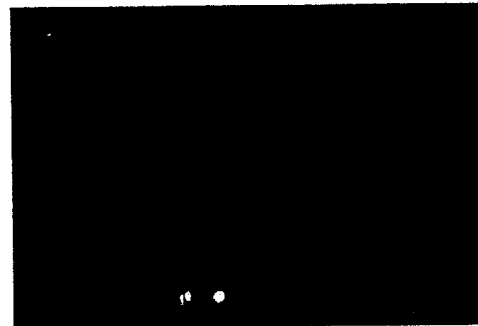


Figure 8e: 2 cm/s spread

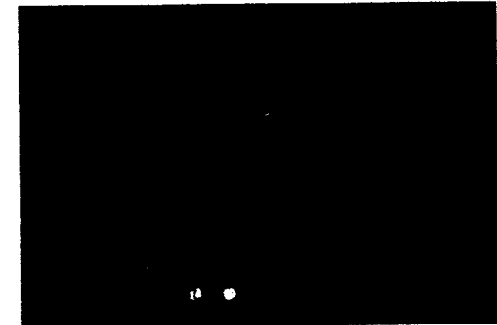


Figure 8f: 2 cm/s full spread

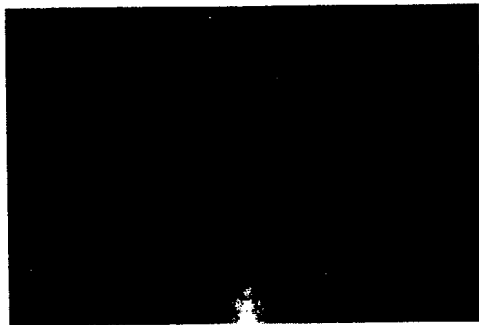


Figure 8g: 6.5 cm/s after ignition

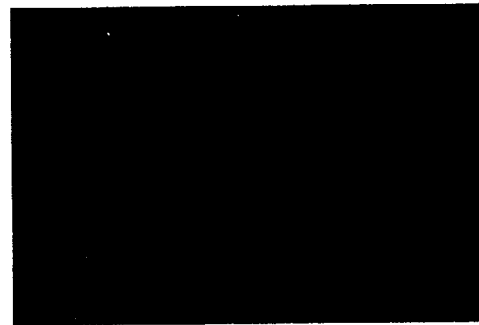


Figure 8h: 6.5 cm/s spread



Figure 8i: 6.5 cm/s full spread

Figure 8 Flame spread patterns at three different flow velocities in three-dimensional configuration (Flow from right)

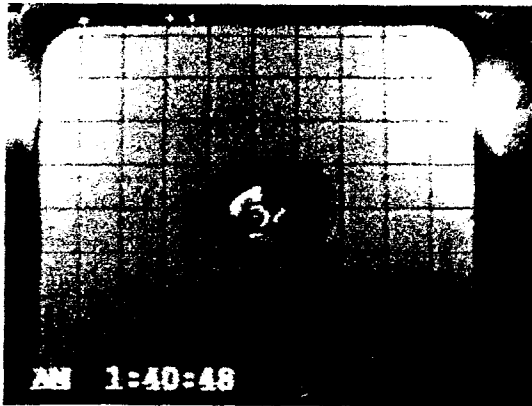


Figure 9a: 0.5 cm/s after ignition

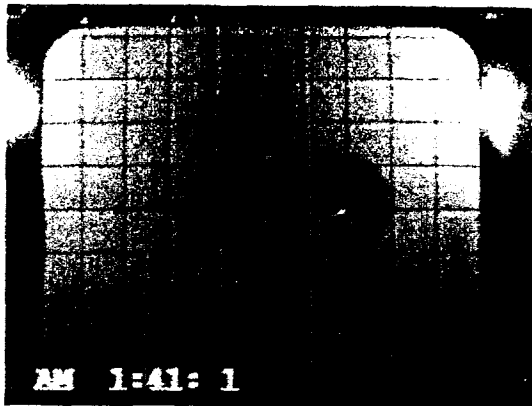


Figure 9b: 0.5 cm/s spread

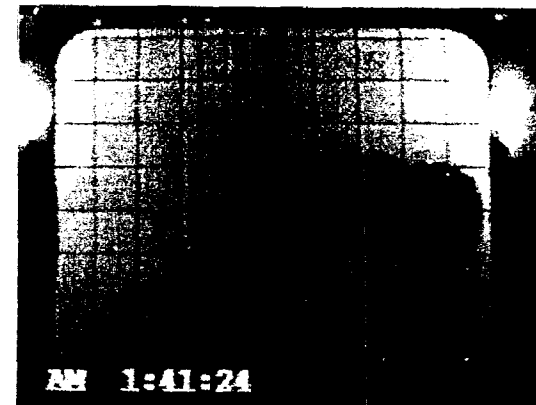


Figure 9c: 0.5 cm/s fully spread upstream

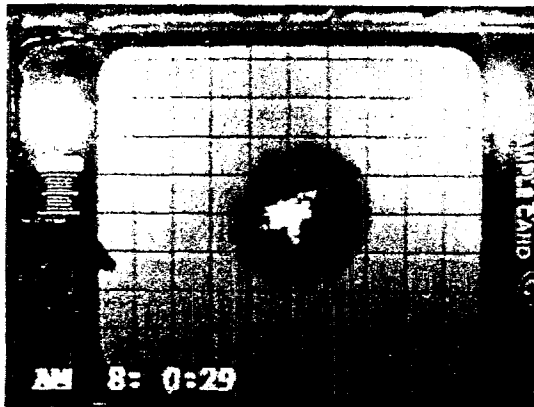


Figure 9d: 2 cm/s after ignition

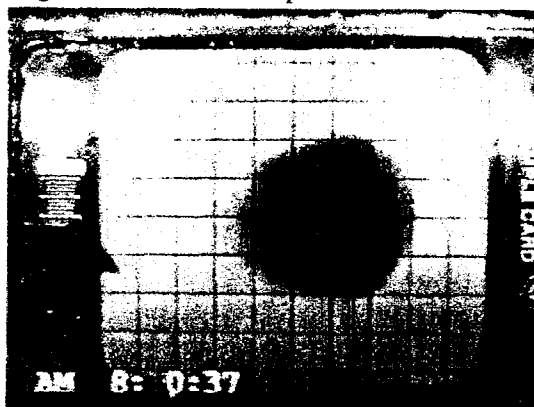


Figure 9e: 2 cm/s spread

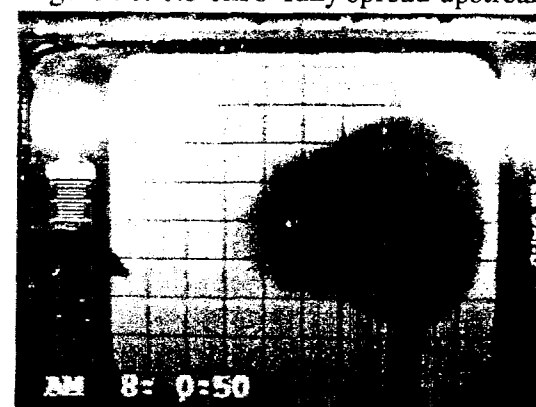


Figure 9f: 2 cm/s fully spread upstream



Figure 9g: 6.5 cm/s after ignition

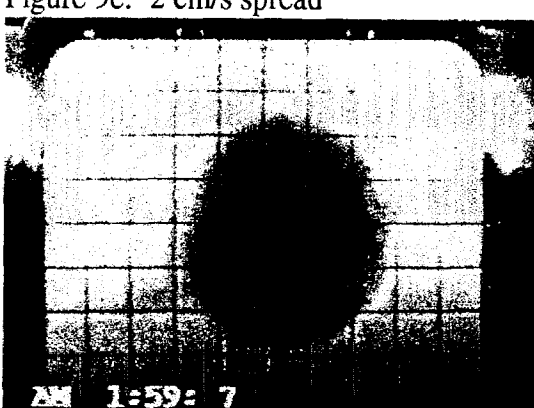


Figure 9h: 6.5 cm/s spread



Figure 9i: 6.5 cm/s fully spread upstream

Figure 9 Char growth Patterns in the three-dimensional configuration (Flow from right)

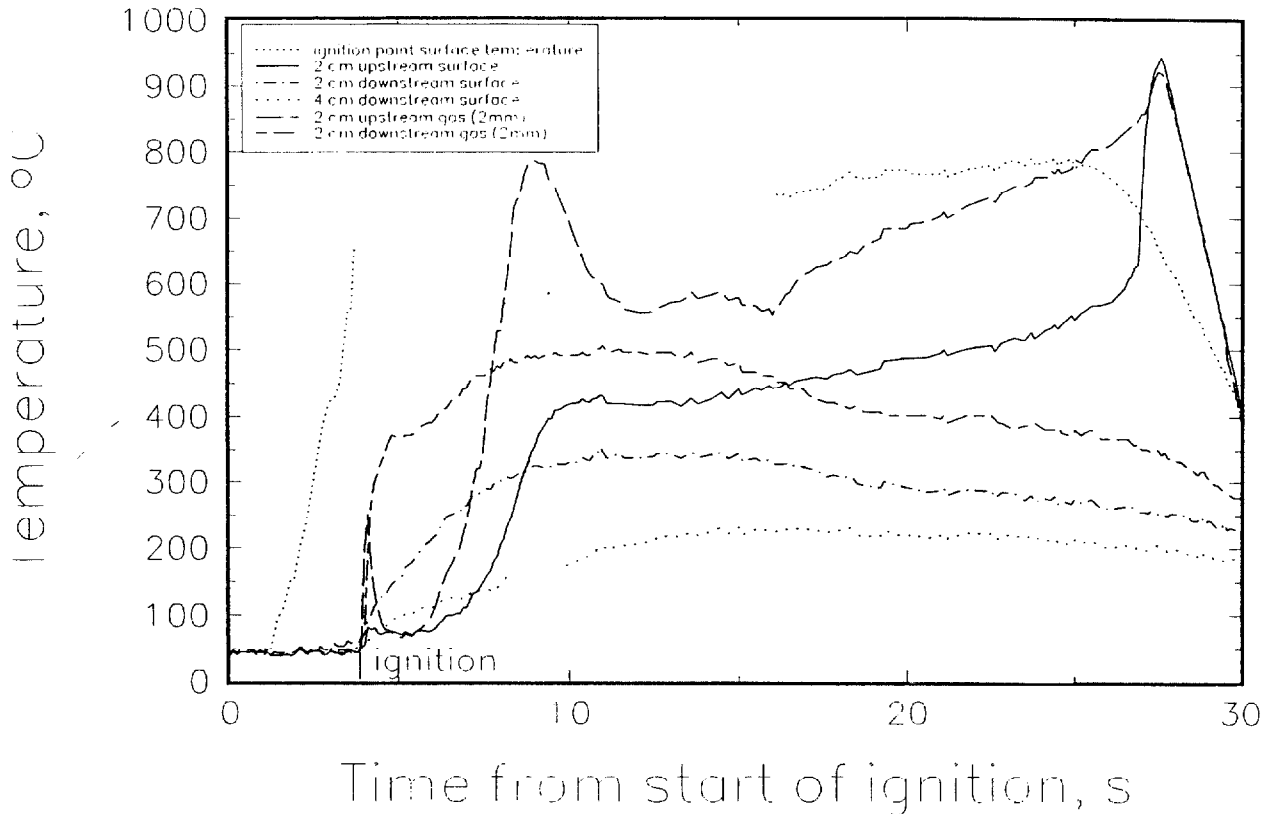


Fig. 10 Temperature histories in three-dimensional configuration, 5 cm/s.

external flow velocity of 5 cm/s are shown in Fig. 10. Time zero was defined as the moment when the power to the lamp was turned on. The delay of temperature increase at the center of the irradiated area was due to the lamp's heat-up time, as discussed above. Unfortunately, the LED display for the center thermocouple was obscured by the reflection of the lamp light and its output could not be read shortly after ignition until the lamp was turned off. A high center temperature indicates that there might be some additional increase in the thermocouple temperature due to the absorption of external radiation from the lamp by the thermocouple bead. Ignition can be recognized as the sudden jumps in the two gas phase temperatures at the locations 2 cm from the center of the irradiated area. The downstream gas phase temperature continued to increase after the ignition due to the flow of hot combustion products but the upstream gas phase temperature dropped rapidly. However, the downstream gas phase temperature went up only to about 500 °C which is much lower than a realistic flame temperature. The behavior of the upstream gas phase temperature indicates that a sudden expansion of flame at ignition momentarily reached to this location but the gas there contracted and the external flow quickly cooled down the local gas temperature. The downstream sample temperatures at the 2 cm and 4 cm locations increased earlier than that at the 2 cm upstream location due to the convecting heating from the hot combustion products flow. However, the downstream sample temperature increased up to only about 350 °C at 2 cm and to about 220 °C at 4 cm. The upstream temperature at 2 cm increased rapidly to about 430 °C and further increase appears to be caused by movement of the thermocouple bead into the gas phase. The first peak of the downstream gas

phase temperature 2 mm above the sample surface at 2 cm was due to the traveling flame front and the second peak was due to the approach of the tail end of the flame. The net energy feedback rate from the traveling downstream flame to the sample surface was calculated with the temperature plot at 2 cm upstream location using the same assumptions described in the two-dimensional configuration. The value is $4.1 \text{ W/cm}^2 \pm 10\%$ for each face of the sample surface (two flames along the two faces of the sample); this is about 25% higher than that in the two-dimensional configuration discussed above. The net energy feedback rates at the two downstream locations are $1.6 \text{ W/cm}^2 \pm 10\%$ and $0.5 \text{ W/cm}^2 \pm 10\%$. These values are also significantly larger than those in the two-dimensional configuration: about 30% and 100%, respectively.

The histories of the char front spreading upstream along the centerline are plotted in Fig.11 using the results shown in Fig.9 to determine the relationship between the location of the char front and

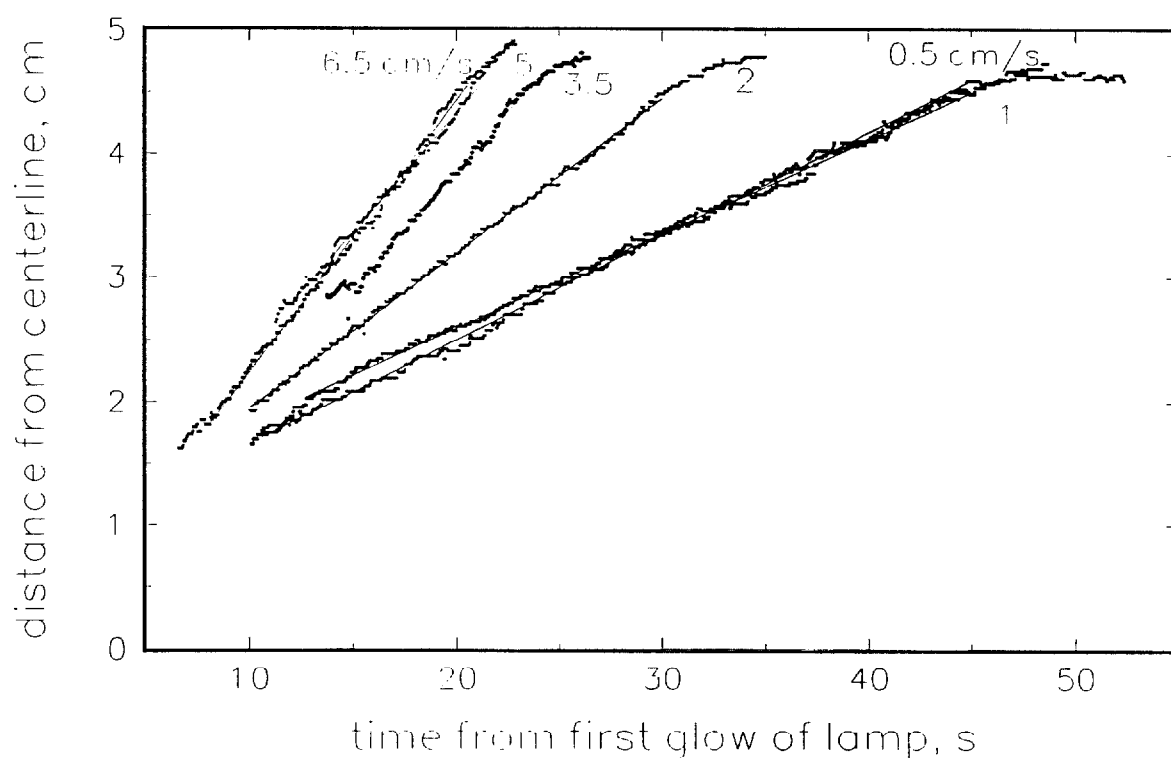


Fig. 11 Upstream char-front location histories in three-dimensional configuration.

time after the initial glow of the ignitor wire. Although the shape of the flame and the curvature of the flame front changed with time, the relationships can be reasonably well fitted by linear equations except when the char front came close to the sample edge. Thus, apparent steady-state-like char front spread rates along the centerline are obtained for each external flow velocity. These apparent steady-state char spread rates are plotted against the external flow velocity in the two- and three-dimensional configurations. The results are shown in Fig.12. Some caution is needed in comparing the results between the two-dimensional configuration and the three-

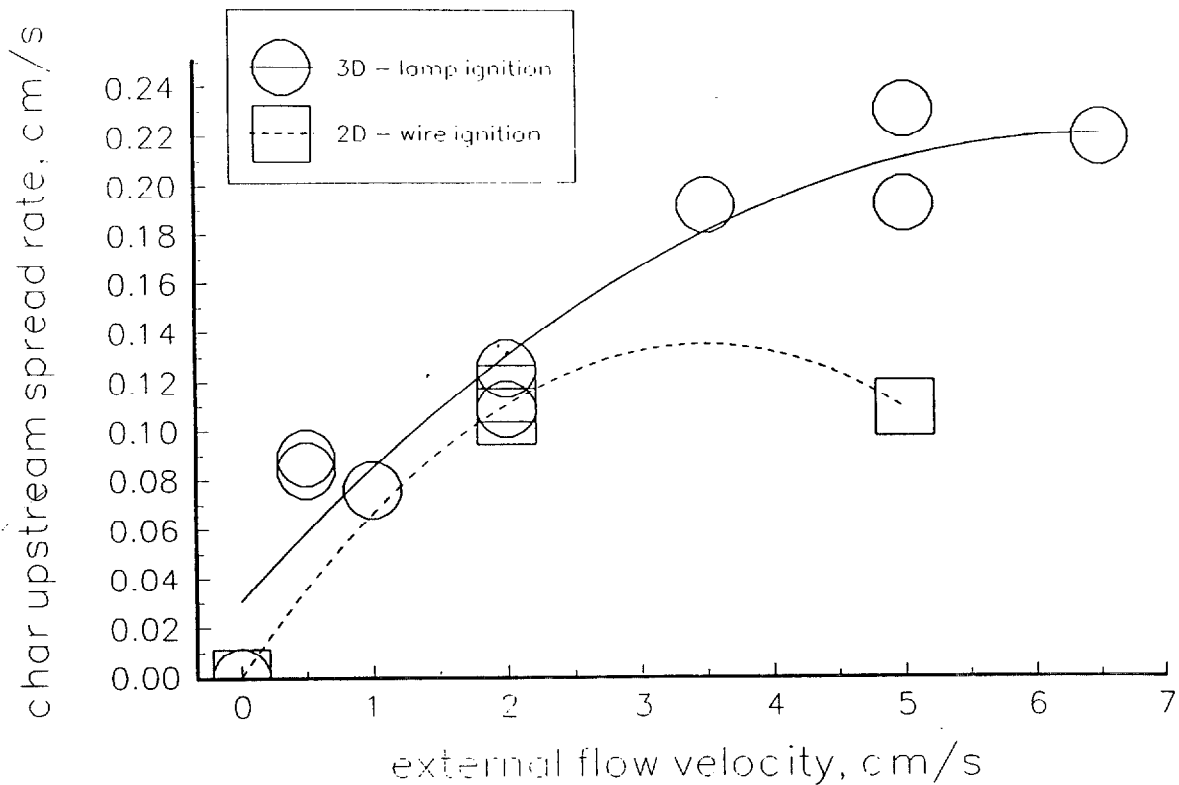


Fig. 12 Char upstream spread rate versus external flow velocity.

dimensional configuration due to the transient nature of the three-dimensional flame and the fact that there is only one data point at 5 cm/s in the two-dimensional configuration. However, it is interesting to note that in the three-dimensional configuration the char spread rate continues to increase with an increase in external velocity and it appears that the maximum spread rate might not have been reached. On the other hand, it appears that the maximum flame might already be reached in the two-dimensional configuration. (The existence of a maximum flame spread with respect to external flow velocity was first demonstrated by Olson.^[17]) Since only four experiments were conducted in the two-dimensional configuration and also since there is some unsteady nature of the char spread rate for the case of 5 cm/s, further experiments are needed to determine the relationship between the spread rate and external flow velocity. If this trend is true, the above discussed higher net energy feedback rate from the flame to the sample surface in the three-dimensional configuration indicates that the three-dimensional flame front might be more intense due possibly to a larger oxygen supply at the curved flame front. In the regime where oxygen supply is a critical rate-controlling process, a curved flame front has a larger area for incoming oxygen to reach. A similar trend of a higher maximum flame spread rate in the three-dimensional configuration versus that in the two-dimensional configuration was also observed in 35% and 50% oxygen concentrations in our drop tower experiments. However, if our explanation is correct, the flame spread rate in the three-dimensional configuration should decrease as the curvature of the flame decreases with an increase in the distance from the ignition area. Although a slow down of spread rate beyond 4 cm from the center is observed, as shown in Fig. 11, it is not clear that this was caused by a more planar flame front or by the flame front moving at a higher flow velocity when the flame got close to the leading edge of the boundary

layer. In order to confirm this trend further, we need to conduct more tests in the two-dimensional configuration, with larger size samples in the three-dimensional configuration, and also at higher external flows.

3.2c Flame spread along the open edges of samples

The flame spread behavior along the open edges of the paper sample was studied using a narrow sample, 4 cm in width, in the same sample holder. Ignition was achieved by the lamp illuminating the center of the sample; initially, the flame spread radially upstream. This behavior is shown in Figs. 13. Once the flame reached the open edges of the sample, the flames at each edge spread much more rapidly than the flame along the center line, as shown in Figs. 13b, 13c, 13e, and 13f. At the open edges of the sample, oxygen supply to the flame (almost 360°) and energy feedback from the flame to the sample (from three sides) are much larger than that for the flame along the center of the sample (about 180° for oxygen supply and only two sides for energy feedback). However, under an external flow velocity of 2 cm/s, it appears that oxygen concentration along the downstream edges was not sufficient due to dilution from the combustion products of upstream flame; flame spread along only the upstream edges. Above an external flow velocity of 3.5 cm/s, oxygen supply to the downstream edges was sufficient and flames spread downstream as well as upstream along the open edges of the sample as shown in Figs. 13e and 13f.

3.3 Smoldering

In RITSI, four smoldering experiments were conducted with ignition initiated at the center of the sample by the lamp. The sample was doped with potassium ions to enhance char formation and char oxidation (4.2 weight % $\pm 5\%$ in spatial non-uniformity). Although a ring-shaped smoldering front was initially observed in normal gravity (the-ring shaped front gradually deformed due to induced buoyant flow from the hot smoldering surface), unexpected, very complex finger-shaped char patterns with localized smoldering fronts at the finger tips were observed in microgravity; such patterns are seen in Figs. 14. In these pictures, the white spots are the localized smoldering fronts. The direction of growth of the char pattern was mainly upstream; higher external flow velocity tends to increase the number of localized smoldering fronts, the number of fingers, and also the frequency of bifurcations from each finger. At present it is not clear what caused this complex pattern. One possible explanation is that there is some non-uniformity in sample thickness and the concentration of potassium ions (doped to the sample to enhance smoldering) in the filter paper. Since potassium ions were heavily doped into the samples (more than needed to make sure that smoldering rate does not depend on the ion concentration), we believe that this phenomenon was not caused by a non-uniformity ($\pm 5\%$) in ion concentration in the sample. Since smoldering induces roughly 20 cm/s buoyancy induced flow in normal gravity, it might be that any non-uniformity of the sample tends to be suppressed in normal gravity. In microgravity, however, it appears that a flow velocity up to 6.5 cm/s does not suppress it. Another possible explanation is that this is a unique instability phenomenon which could occur only at low flow velocities below the buoyancy induced flow velocity such as is the case under microgravity conditions.

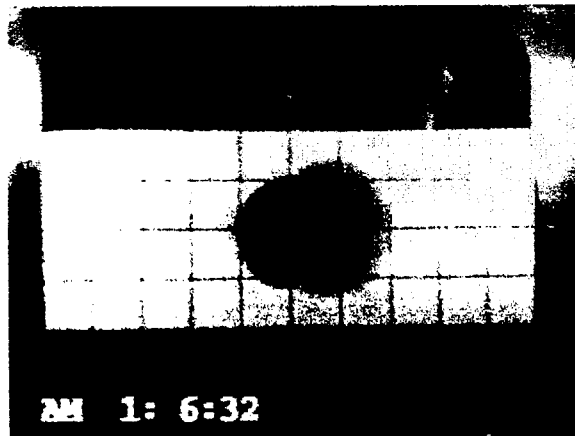


Figure 13a: 2 cm/s post ignition

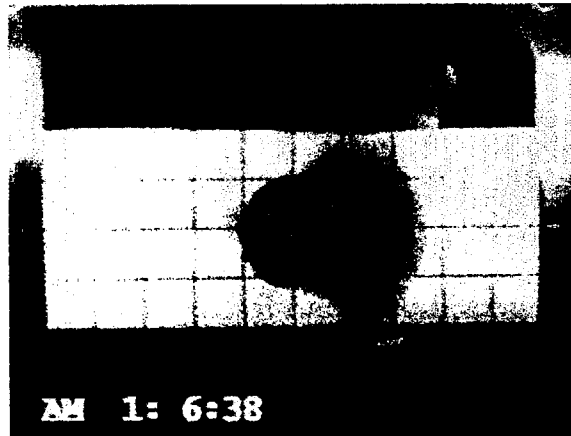


Figure 13b: 2 cm/s enhanced edge spreading

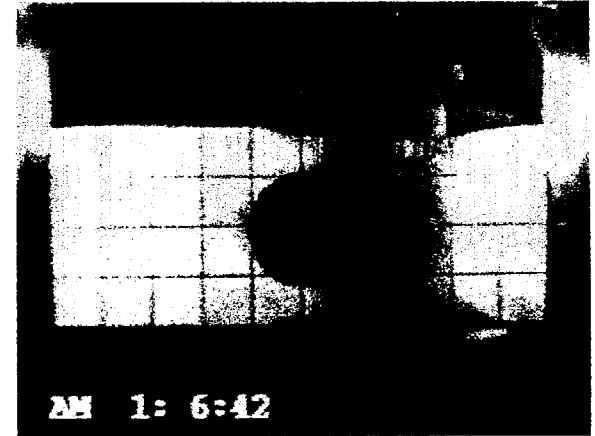


Figure 13c: 2 cm/s upstream spread only

113

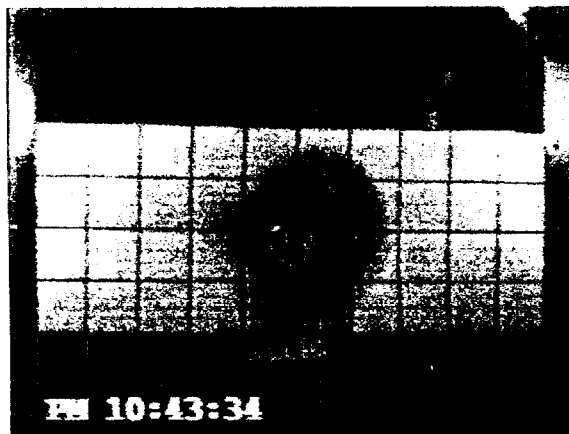


Figure 13d: 5 cm/s post ignition

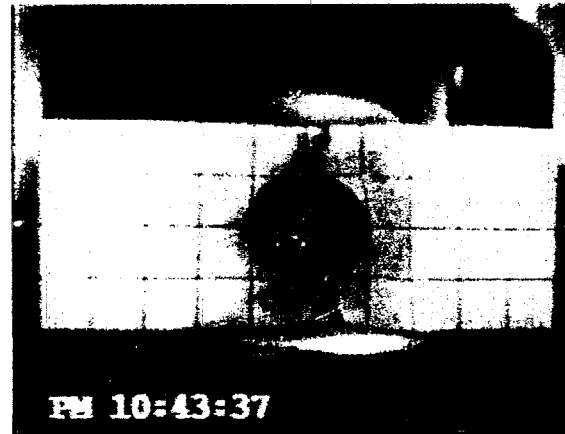


Figure 13e: 5 cm/s enhanced edge spreading



Figure 13f: 5 cm/s bidirectional edge spread

Figure 13 Flame spread patterns along open edges (Ignition was initiated at the center, Flow from right).

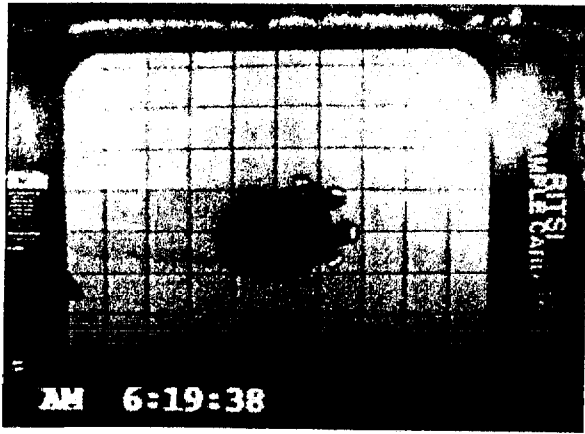


Figure 14a: 0.5 cm/s flow test, just after ignition



Figure 14b: 0.5 cm/s flow test, later in the burn

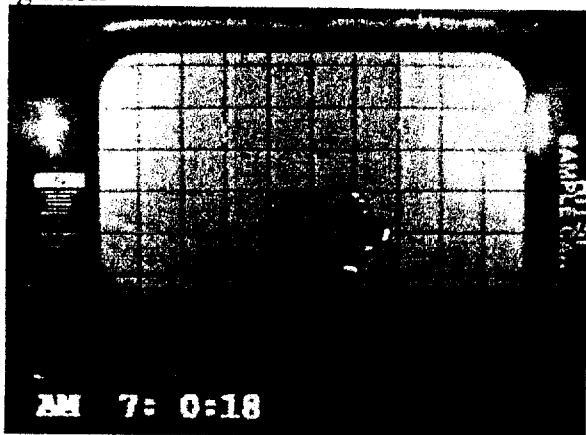


Figure 14c: 2 cm/s flow test, just after ignition

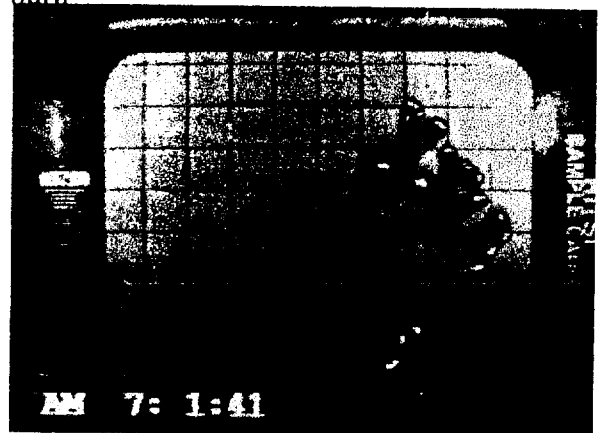


Figure 14d: 2 cm/s flow test, later in the burn



Figure 14e: 6.5 cm/s flow test, just after ignition



Figure 6: 6.5 cm/s flow test, later in the burn

Figure 14 Smoldering char growth patterns at different flow velocities. (Flow from right)

4. Summary

Non-piloted ignition by external thermal radiation of a cellulosic paper tends to occur more easily in microgravity than in normal gravity. Downstream flame spread was never observed in the two-dimensional configuration exposed to external flow velocity of up to 5 cm/s, when ignition was initiated locally in the middle part of a thin paper. This was presumably due to lack of oxygen due to the dilution of combustion products from the upstream flame (oxygen shadow effect). In the three-dimensional configuration, when ignition was initiated locally in a small circle in the center of the sample, flame spread was again mainly upstream. At the lowest flow (0.5 cm/s) for sustained spread, the flame remained a very small hemisphere that propagated directly upstream without any lateral spread. At 1 cm/s, the flame fanned out slightly as it propagated upstream. The fan angle increased with flow velocity. At 6.5 cm/s, the flame became horseshoe-shaped. It appears that the three-dimensional flame front (i.e., curved flame front) might be more intense than that in the two-dimensional flame front (planar flame) due to larger oxygen supply to the curved flame front. The peak upstream flame spread rate in the two-dimensional configuration tends to occur at lower external flow velocity than that in the three-dimensional configuration. The shape of the upstream flame front might have important effects on the strength of the flame front and upstream flame spread rate.

Flame spread much faster along open edges of a thin paper sample than along the sample surface. At the external flow velocity of 2 cm/s, flame spread along open edges only upstream while, above 3.5 cm/s, flame spread along open edges downstream as well as upstream.

An unexpected, complex surface smoldering char growth pattern was observed when localized smoldering was initiated at the center of the sample by a lamp. Instead of a ring-like smoldering front as is observed in normal gravity, finger-shaped char growth pattern with several localized smoldering fronts was observed. Generally, the char growth pattern was mainly upstream. The number of localized smoldering fronts, the number of fingers, and the frequency of bifurcations of the finger increased with an increase in external flow velocity. At present, it is not clear what causes this complex char growth pattern.

Acknowledgment

This work is funded by the NASA Microgravity Science Program under the Inter-Agency Agreement No. C-32001-R.

References

1. Friedman, R. and Sacksteder, K.r. "Fire Behavior and Risk Analysis in Spacecraft" NASA TM100944, December 1988.
2. Smith, R. and Kashiwagi, T. *J. Applied Fire Sci.* 1-2: 103-113(1990-91).
3. Kashiwagi, T. *Fire Safety J.* 3: 185-200(1981).

4. Kashiwagi, T. *Combust. Flame* 34: 231-244(1979).
5. Muto, N., Hirano, T. and Akita, K. *Seventeenth Symposium (International) on Combustion*, The Combustion Institute, Pittsburgh, 1183-1190(1978).
6. Akita, K. in "Aspects of Degradation and Stabilization of Polymers" (H.H.G. Jellinek, Ed.), Elsevier Scientific, 1978, Chapt.10.
7. Bhattacharjee, S and Altenkirch, R.A. *Twenty-Third Symposium (International) on Combustion*, The Combustion Institute, Pittsburgh, 1627-1633(1990).
8. Frey, A.E. and Tien, J.S., *Combust. Flame*, 36: 263-289(1979).
9. Kashiwagi, T. *Combust. Sci. Tech.* 8: 225-236(1974).
10. Kindelan, M. and Williams, F. *Combust. Sci. Tech.* 16: 47-58(1977).
11. Krishnamurthy, L. *Acta Astronaut.* 3: 935 (1976).
12. Amos, B. and Fernandez-Pello, A.C. *Combust. Sci. Tech.* 62: 331-343(1988)
13. Di Blasi, C., Crescitelli, S. and Russo, G. *Fire Safety Science- Proceedings of the Second International Symposium*, p119-128(1989).
14. McGrattan, K.B., Kashiwagi, T., Baum, H.R., and Olson, S.L., *Combust. Flame*, 106: 377-391(1996).
15. Kashiwagi, T., and Nambu, H., *Combust. Flame*, 88: 345-368(1992).
16. Kashiwagi, T., McGrattan, K.B., Olson, S.L., Fujita, O., Kikuchi, M., and Ito, K. "Effects of Slow Wind on Localized Radiative Ignition and Transition to Flame Spread in Microgravity", to appear in *Twenty-Six Symposium (International) on Combustion*, The Combustion Institute.
17. Olson, S.L., *Combust. Sci. Technol.*, 76: 233-249(1991).

Table 1 Test Matrix

Test No.	Configuration	Flow cm/s	Ignitor	Notes
1	Flaming 2D	5	Wire	
2	Flaming 3D	5	Lamp	
3	Flaming 3D	5	Lamp	
4	Flaming 2D	2	Wire	
5	Flaming 2D	0	Wire	No transition
6	Flaming 3D	2	Lamp	
7	Flaming 3D	0.5	Lamp	
8	Flaming 3D	2	Lamp	Spread along open edges
9	Smolder 3D	5	Lamp	Smoldering
10	Smolder 3D	0.5	Lamp	Smoldering
11	Flaming 3D	3.5	Lamp	
12	Flaming 2D	2	Wire	
13	Flaming 3D	1	Lamp	
14	Smolder 3D	2	Lamp	Smoldering
15	Smolder 3D	6.5	Lamp	Smoldering
16	Flaming 3D	2	Lamp	
17	Flaming 3D	5	Lamp	Spread along open edges
18	Flaming 3D	0	Lamp	No transition
19	Flaming 3D	2	Lamp	Spread along open edges
20	Flaming 3D	1	Lamp	No 35 mm camera
21	Flaming 3D	0.5	Lamp	No 35 mm camera
22	Flaming 3D	6.5	Lamp	
23	Flaming 3D	5	Lamp	Spread along corner
24	Flaming 3D	3.5	Lamp	Spread along open edges
25	Flaming 3D	5	Lamp	Spread along corner